HHS Public Access

Author manuscript

Bioconjug Chem. Author manuscript; available in PMC 2022 July 21.

Published in final edited form as:

Bioconjug Chem. 2021 July 21; 32(7): 1306–1314. doi:10.1021/acs.bioconjchem.0c00649.

ImmunoPET of CD146 in Orthotopic and Metastatic Breast Cancer Models

Cuicui Li[#],
Department of Nuclear Medicine, Peking University First Hospital, Beijing, China 100034

Lei Kang[#],
Department of Nuclear Medicine, Peking University First Hospital, Beijing, China 100034;

Departments of Radiology and Medical Physics, University of Wisconsin-Madison, Madison, Wisconsin 53705, United States;

Kevin Fan,
Departments of Radiology and Medical Physics, University of Wisconsin-Madison, Madison, Wisconsin 53705, United States

Carolina A. Ferreira,
Department of Biomedical Engineering, University of Wisconsin-Madison, Madison, Wisconsin 53705, United States

Kaelyn V. Becker,
Departments of Radiology and Medical Physics, University of Wisconsin-Madison, Madison, Wisconsin 53705, United States

Nan Huo,
Department of Medical Molecular Biology, Beijing Institute of Biotechnology, Beijing, China 100850

Hanxiao Liu,
Department of Oncology, Harbin Medical University Affiliated Cancer Hospital, Harbin, China 150081

Yunan Yang,
Departments of Radiology and Medical Physics, University of Wisconsin-Madison, Madison Wisconsin 53705, United States

Jonathan W. Engle,

Corresponding Authors: Lei Kang – Department of Nuclear Medicine, Peking University First Hospital, Beijing, China 100034; Departments of Radiology and Medical Physics, University of Wisconsin-Madison, Madison, Wisconsin 53705, United States; Phone: 8610-8357-5252; kanglei@bjmu.edu.cn; Fax: 8610-8357-2914, **Xiaojie Xu –** Department of Medical Molecular Biology, Beijing Institute of Biotechnology, Beijing, China 100850; Phone: 8610-6693-1830; miraclexxj@126.com; Fax: 8610-6824-8045, **Dawei Jiang –** Departments of Radiology and Medical Physics, University of Wisconsin-Madison, Madison, Wisconsin 53705, United States; Department of Nuclear Medicine, Union Hospital, Tongji Medical College, Huazhong University of Science and Technology, Wuhan, China 430022; daweijiang@hust.edu.cn, **Weibo Cai –** Departments of Radiology and Medical Physics and Department of Biomedical Engineering, University of Wisconsin-Madison, Madison, Wisconsin 53705, United States; Phone: 608–262-1749; wcai@uwhealth.org; Fax: 608-265-0614.

Complete contact information is available at: https://pubs.acs.org/10.1021/acs.bioconjchem.0c00649

The authors declare no competing financial interest. All applicable international, national, and/or institutional guidelines for the care and use of animals were followed.

Departments of Radiology and Medical Physics, University of Wisconsin-Madison, Madison, Wisconsin 53705, United States

Rongfu Wang,
Department of Nuclear Medicine, Peking University First Hospital, Beijing, China 100034

Xiaojie Xu,
Department of Medical Molecular Biology, Beijing Institute of Biotechnology, Beijing, China 100850;

Dawei Jiang,
Departments of Radiology and Medical Physics, University of Wisconsin-Madison, Madison, Wisconsin 53705, United States;

Department of Nuclear Medicine, Union Hospital, Tongji Medical College, Huazhong University of Science and Technology, Wuhan, China 430022;

Weibo Cai
Departments of Radiology and Medical Physics and Department of Biomedical Engineering, University of Wisconsin-Madison, Madison, Wisconsin 53705, United States;

[#] These authors contributed equally to this work.

Abstract

The overexpression of CD146 in breast cancer is considered a hallmark of tumor progression and metastasis, particularly in triple negative breast cancer. Aimed at imaging differential CD146 expressions in breast cancer, a noninvasive method for predictive prognosis and diagnosis was investigated using a ^{64}Cu-labeled CD146-specific monoclonal antibody, YY146. CD146 expression was screened in human breast cancer cell lines using Western blotting. Binding ability was evaluated using flow cytometry and immunofluorescent staining. YY146 was conjugated with 1,4,7-triazacyclononane-triacetic acid (NOTA) and radiolabeled with ^{64}Cu following standard procedures. Serial PET or PET/CT imaging was performed in orthotopic and metastatic breast cancer tumor models. Biodistribution was performed after the final time point of imaging. Finally, tissue immunofluorescent staining and hematoxylin and eosin (H&E) staining were performed on tumor tissues. The MDA-MB-435 cell line showed the highest CD146 expression level, whereas MCF-7 had the lowest level at the cellular level. ImmunoPET showed that MDA-MB-435 orthotopic tumors had high and clear radioactive accumulation after the administration of ^{64}Cu-NOTA-YY146. The tumor uptake of ^{64}Cu-NOTA-YY146 in MDA-MB-435 was significantly higher than that in MCF-7 and nonspecific IgG control groups ($P < 0.01$). Biodistribution verified the PET imaging results. For metastatic models, ^{64}Cu-NOTA-YY146 allowed for the visualization of high radioactivity accumulation in metastatic MDA-MB-435 tumors, which was confirmed by ex vivo biodistribution of lung tissues. H&E staining proved the successful building of metastatic tumor models. Immunofluorescent staining verified the differential expression of CD146 in orthotopic tumors. Therefore, ^{64}Cu-NOTA-YY146 could be used as an immunoPET probe to visualize CD146 in the breast cancer model and is potentially useful for cancer diagnosis, prognosis prediction, and monitoring therapeutic response.

Graphical Abstract

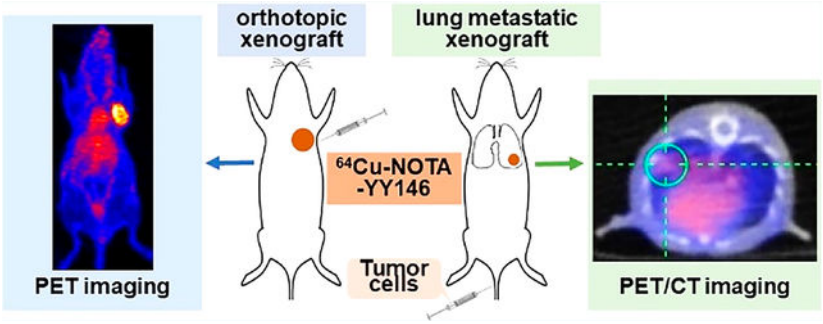

INTRODUCTION

Breast cancer is a disease with high morbidity and mortality. The latest cancer statistics report reveals that breast cancer is the second-leading cause of female cancer deaths (about 15%) in the United States. In 2020 alone, it is estimated that there will be 279,100 new breast cancer cases and 42,690 deaths.[1] Early diagnosis, treatment, and monitoring of therapeutic effects are still the main means for breast cancer. Among various noninvasive diagnostic methods, imaging is an indispensable method. Mammography is inexpensive and well-tolerated, but it has limitations relating to insensitivity to small lesions and high radiation dosages.[2] Ultrasound diagnosis is widely used without radiation, but it is not specific for the differential diagnosis of benign and malignant breast nodules.[3] Magnetic resonance imaging (MRI) and positron emission tomography (PET) have high sensitivity in breast cancer diagnosis, and single photon emission computed tomography (SPECT) provides an important value in bone metastasis.[4–6] However, these conventional imaging methods lack specificity. With the development of technology, the treatment of cancer has become increasingly personalized, with precision medicine being seen as the future developmental trend. Therefore, new and specific imaging methods are needed for tumor diagnosis, prognosis prediction, and monitoring of therapeutic effects.

ImmunoPET is a developed specific imaging method using radionuclide-labeled specific monoclonal antibodies (mAbs) or fragments for imaging. This method noninvasively shows the expression and distribution of targeted antigens at the living level.[7–9] CD146 is a transmembrane glycoprotein cell adhesion molecule with a molecular weight of about 110 kDa, first found in malignant melanoma, which is also known as melanoma cell adhesion molecule (MCAM) or MUC18.[10] CD146 has been proven to be associated with poor breast cancer prognosis and is generally expressed at high levels in high-grade, estrogen receptor (ER) negative, progesterone receptor (PR) negative, or triple (ER/PR/human epidermal growth factor receptor 2 (HER2)) negative breast cancer (TNBC).[11,12] Besides, CD146 expression is also related to the resistance of endocrine therapy.[13,14] When the expression level of CD146 in the primary breast tumor is high, the overall survival (OS), recurrence-free survival (RFS) and distant metastasis-free survival (DMFS) are significantly reduced.[13]

Therefore, the imaging of differential CD146 expression in breast cancer may provide a noninvasive method in cancer diagnosis, staging, prognosis prediction, and efficacy evaluation. Our team previously developed CD146-specific mAb YY146, which had been

studied in lung cancer, glioblastoma, melanoma, and hepatocellular carcinoma, with immunoPET imaging being successfully performed with high-quality images.[5–19] However, whether radiolabeled YY146 could be effectively used in breast cancer, especially metastatic models, is still unknown. Therefore, in this study, we developed a ^{64}Cu-labeled YY146 radioactive tracer and evaluated its application in the noninvasive imaging of differential CD146 expression in orthotopic and lung metastatic breast cancer models, which is the first instance of immunoPET imaging of CD146 in breast cancer to our knowledge.

MATERIALS AND METHODS

Cell Culture.

Five breast cancer cell lines (MDA-MB-435, ZR-75–30, SKBR3, MCF-7, and MDA-MB-231) were purchased from American Type Culture Collection (ATCC). The cells were cultured in RPMI 1640 medium supplemented with 10% fetal bovine serum (FBS, Invitrogen) and 1% penicillin/streptomycin (Invitrogen) with 5% CO_2 partial pressure at 37 °C. When the confluence of cells was 75–90%, cells were used for in vitro or in vivo experiments.

Orthotopic and Metastatic Tumor Models.

Animal studies were approved by the Wisconsin University Institutional Animal Care and Use Committee and Peking University First Hospital (No. 201859). BALB/c nude mice (4–6 weeks old, Envigo) were used to establish xenograft tumor models. Approximately 1×10^7 cells were resuspended in 200 μL of Matrigel (Invitrogen) and then injected subcutaneously in the right upper mammary fat pad of the mice to construct orthotopic tumor models. Approximately 1×10^6 cells were resuspended in 200 μL of phosphate buffer saline (PBS) and injected via tail vein to construct lung metastatic tumor models. The health status and tumor volume of the mice were monitored every other day.

Western Blotting.

Western blotting was performed following the standard protocols.[20] Collected proteins were loaded in 4–12% Bolt Bis-Tris Plus gel (ThermoFisher Scientific) and electrophoresed for 60 min under 120 V at 4 °C. The protein was transferred to the nitrocellulose membrane using the iBlot 2 system (ThermoFisher Scientific) at 160 mA for 30 min. The membrane was blocked with Odyssey blocking buffer (LI-COR Biosciences) at room temperature (RT) for 1 h. Mouse anti-human monoclonal CD146 primary antibody (Santa Cruz) was diluted to 1:100, and rabbit anti-human β-actin (LI-COR Biosciences) primary antibody was diluted to 1:400. The donkey anti-mouse IRDye 800CW and goat anti-rabbit IRDye 680RD (LI-COR Biosciences) secondary antibodies were diluted to 1:1500.After the incubation, the membrane was scanned using the LI-COR Odyssey infrared imaging system.

Flow Cytometry.

The binding capacity and specific immunoreactivity of YY146 in breast cancer cell lines were tested by flow cytometry. Cells were harvested and resuspended in cold PBS buffer (pH 7.4) containing 1% BSA at 1×10^6 cells/tube (200 μL). YY146 and nonspecific control IgG were labeled with NHS-fluorescence (NHS-FITC, ThermoFisher) as previously

described.[8] FITC-YY146 was incubated with MDA-MB-435 cells for 1 h at RT, whereas FITC-IgG and FITC only were used as control groups. In the blocking experiment, 500 μg/mL (50 folds), 200 μg/mL (20 folds), and 100 μg/mL (10 folds) of YY146 were incubated with MDA-MB-435 cells for 1 h before the incubation of FITC-YY146 (30 min at RT). All cells were washed twice with cold PBS and then analyzed using LSRFortessa cell analyzer (BD Biosciences). Mean fluorescence intensities were processed by FlowJo analysis software (Tree Star, USA).

Cell Immunofluorescent Staining.

MDA-MB-435 cells were incubated with YY146 at 10 μg/mL overnight when the cell density was 40–60% cultured in six-well plates. The cells were washed with cold PBS three times and then incubated with rabbit anti-mouse secondary antibodies labeled with AF488 (Alexa Fluor 488) at RT for 30 min. Afterward, the cells were washed three times with cold PBS again and treated with DAPI (4',6-diamidino-2-phenylindole, Vector Laboratories) containing hard mount medium. Imaging was performed using a Nikon confocal system (A1RS). MCF-7 cells were treated in the same way as a negative control group.

Conjugation and Radiolabeling.

YY146 was preserved in our laboratory.[19] Details of 1,4,7-triazacyclononane-1,4,7-triacetic acid (NOTA, Macrocyclic) conjugation and ^{64}Cu ($t_{1/2}$ = 12.7 h) labeling of YY146 have been reported previously.[7] In brief, YY146 and NOTA were first incubated in a carbonate buffer (pH 9.2) at a molar ratio of 1:20 and shaken for 2 h at RT. Then, a PD-10 column (GE Healthcare) was used to purify NOTA-YY146 with PBS (pH 7.0) as a mobile phase. Subsequently, the purified NOTA-YY146 was incubated with $^{64}CuCl_2$ in a sodium acetate buffer (pH 4.5–5.5) at 37 °C for 1 h under constant shaking. The ratio of YY146 and radionuclide was not below 25 μg/mCi. Then, ^{64}Cu-NOTA-YY146 was purified via PD-10 columns. Radiochemical purity was evaluated by radio-thin-layer chromatography (radio-TLC), using ethylene diamine tetraacetic acid (EDTA, 50 mM, pH 4.5) as the mobile phase. Nonspecific human IgG (ThermoFisher Scientific) was prepared as a nonspecific control tracer via similar methods as described above.

ImmunoPET, PET/CT Imaging, and Quantitative Analysis.

For orthotopic models, mice were injected with 5–10 MBq of ^{64}Cu-NOTA-YY146 (~200 μL) per mouse via the tail vein. The mice were anesthetized with 2% isoflurane and placed in an Inveon micro-PET/CT scanner (Siemens). Small animal PET scans were performed at 4 h, 12, 24, and 48 h after the injection of ^{64}Cu-NOTA-YY146 in orthotopic xenograft tumor models. PET/CT scanning was performed in lung metastatic tumor models at 48 h. At least 20 million coincidence events were collected per mouse for PET scanning. CT was conducted at the following parameters: energy window 350–650 keV, time window 3.43 ns, axial resolution 1.5 mm. All images were reconstructed using the Inveon Acquisition Workplace (Siemens). Quantitative region of interest (ROI) analysis was performed on PET images after attenuation correction. Radioactive uptake of tumors and normal tissues was presented as the percentage of injected dose per gram (%ID/g). Besides, ex vivo PET imaging was performed on the ablated lung tissues from metastatic tumor models.

Ex Vivo Biodistribution Studies.

After the terminal imaging time point (48 h) in orthotopic xenograft tumor models, the mice were euthanized. Tumors and major organs including the heart, liver, spleen, lung, kidney, stomach, intestine, pancreas, tail, skin, muscle, bone, brain, and blood were all collected and weighed. An automatic gamma counter (PerkinElmer) was used to measure the radioactivity counts. Biodistribution data was presented as %ID/g. For metastatic models, the whole lungs were removed for the measurement of biodistribution data using the same method.

Hematoxylin and Eosin (H&E) Staining.

The lungs of metastatic tumor models were harvested after PET/CT imaging, and the mice were euthanized using carbon dioxide. After collecting the lung, it was fixed with 4% paraformaldehyde (PFA) for 24 h and then placed in 50% alcohol for longterm storage. The lung tissue was embedded in paraffin and sectioned with a thickness of 5 μm. Before H&E staining, the lungs were warmed up at 50–60 °C for at least 40 min. Dimethylbenzene and alcohol of different concentrations were then used to dewax, with each process taking roughly 5 min. After that, the slices were left to stand for 5 min in distilled water. After the slices were dyed in hematoxylin for 1–5 min, they were placed in distilled water for 10–30 min until they turned blue. Eosin was dyed for 1–5 min and then dehydrated in different concentrations of ethanol and dimethylbenzene in sequence, with each process taking about 1 min. Finally, the slices were sealed with neutral resin adhesive. Images were collected using a Nikon microscope.

Tissue Immunofluorescent Staining.

Tissue immunofluorescent staining was performed to evaluate CD146 and CD31 expression in orthotopic tumor models according to established procedures.[21,22] The tumor was quickly removed after the terminal imaging time point (48 h) and prepared into slides at 5 μm. Frozen slides were fixed with cold acetone for 10 min and dried in air for 30 min. Tissue sections were then rinsed with PBS and blocked with 10% donkey serum at 25 °C for 60 min. Next, the slides were incubated with YY146 (10 μg/mL) and rat anti-mouse CD31 primary antibody (1:100, BD BioSciences) at 4 °C overnight. After rinsing with PBS, the slides were stained with AF488-labeled goat anti-mouse antibody and Cy3-labeled donkey anti-rat antibody. A hard mount medium (Vector Laboratories) was used to apply coverslips to each slide for fluorescence microscopy with DAPI. All images were acquired using an A1R confocal microscope (Nikon).

Statistical Analysis.

All quantitative data were presented as means ± standard deviation (SD). Repeated-measures ANOVA and student's t-test were used for comparisons among groups. P values less than 0.05 were considered statistically significant.

RESULTS

Cellular Evaluation of CD146 Expression and Binding Affinity Test.

Western blotting showed that MDA-MB-435 cells expressed the highest level of CD146 while MCF-7 cells expressed the lowest level. CD146 was moderately expressed in ZR-75–30, SKBR3, and MDA-MB-231 cell lines (Figure 1A). In flow cytometry, compared with FITC only and FITC-IgG control groups, FITC-YY146 showed a strong shift of peak after incubated with MDA-MB-435 cells and was blocked using >10-fold concentration of YY146. These results indicated that the binding between FITC-YY146 and MDA-MB-435 cells was specific (Figure 1B). The cell immunofluorescent staining was performed on the MDA-MB-435 and MCF-7 cells (Figure 1C). MDA-MB-435 cells showed strong CD146 fluorescence signals around the cell membrane, whereas MCF-7 cells had weak signals. Therefore, the MDA-MB-435 cell line was chosen as the CD146-overexpressed model and MCF-7 as the low-expressed model. The schematic diagram of this study is displayed in Figure 1D. ImmunoPET and PET/CT imaging were performed on orthotopic and metastatic tumor models, respectively, to evaluate the different CD146 expression levels.

ImmunoPET Imaging of Orthotopic Breast Cancer Model.

After conjugated with NOTA, YY146 was successfully labeled with ^{64}Cu with a high labeling efficiency of more than 90% ($n = 4$). The radiochemical purity of ^{64}Cu-NOTA-YY146 exceeded 95%. The maximum intensity projection (MIP) images of the orthotopic tumor models showed that the tumor uptake of ^{64}Cu-NOTA-YY146 in MDA-MB-435 increased over time. The MDA-MB-435 tumor was delineated as early as 12 h after injection of ^{64}Cu-NOTA-YY146, and tracer uptake reached its highest at 48 h. MCF-7 and ^{64}Cu-NOTA-IgG in MDA-MB-435 showed background tracer uptake, confirming the specificity of YY146 to CD146 in vivo (Figure 2). Radioactive uptake was mainly found in the heart, blood, and liver and decreased over time, indicating ^{64}Cu-NOTA-YY146 and ^{64}Cu-NOTA-IgG had favorable blood clearance.

Quantitative ROI analysis (Figure 3A) observed that the tumor uptake of ^{64}Cu-NOTA-YY146 in MDA-MB-435 was high and sustained (>6.05%ID/g) and reached its highest at 48 h post injection (p.i.), about 14.7 ± 1.75%ID/g ($n = 4$). On the contrary, MCF-7 and ^{64}Cu-NOTA-IgG in MDA-MB-435 could not be clearly shown and the highest tumor uptake was only 5.13 ± 0.70 and 5.0 ± 0.70%ID/g, respectively ($n = 3$). The tumor uptake of ^{64}Cu-NOTA-YY146 in MDA-MB-435 was significantly different from that of MCF-7 and ^{64}Cu-NOTA-IgG in MDA-MB-435 ($P < 0.01$). There was no significant difference in tumor uptake between ^{64}Cu-NOTA-YY146 in MCF-7 and ^{64}Cu-NOTA-IgG in MDA-MB-435 ($P > 0.05$). Tracer accumulation in the heart, liver, and kidney gradually decreased over time. The heart uptake of ^{64}Cu-NOTA-YY146 in MDA-MB-435 was significantly lower than that in MCF-7 ($P < 0.05$), whereas liver and kidney uptake had no significant difference ($P > 0.05$). The tumor/blood and tumor/liver ratios of ^{64}Cu-NOTA-YY146 in MDA-MB-435 were also significantly higher than the other two control groups ($P < 0.01$) (Figure 3B). These semiquantitative results indicated that ^{64}Cu-NOTA-YY146 could specifically evaluate CD146 expression level in vivo.

Ex Vivo Biodistribution of Orthotopic Models.

The ex vivo biodistribution result was consistent with the in vivo immunoPET imaging (Figure 3C). The tumor uptake of ^{64}Cu-NOTA-YY146 in MDA-MB-435 was 18.09 ± 3.51%ID/g (n = 4), which had significant differences from MCF-7 and ^{64}Cu-NOTA-IgG in MDA-MB-435 (n = 3, 3.08 ± 0.98 and 4.47 ± 0.55%ID/g, P < 0.01, respectively). There was no statistical difference in the radioactive uptake of other organs among the three groups (P > 0.05) except tumors. All tumor-bearing mice showed similar blood radioactivity uptake, indicating that the antibody was stable during circulation. The decrease of radioactivity uptake in liver, kidney, and spleen was smaller than those of other organs p.i., indicating that YY146 might be cleared mainly through the hepatobiliary circulatory and urinary systems.

PeT/CT Imaging of Lung Metastatic Models.

PET/CT imaging was performed at 48 h p.i. of ^{64}Cu-NOTA-YY146 in lung metastatic tumor models. For both MDA-MB-435 and MCF-7 models, the metastatic lesion in the lung was visualized clearly by CT images, by representing small lung nodules. However, from PET imaging, the lung lesion showed high radioactivity accumulation in MDA-MB-435 models. In comparison, the metastatic lung lesion showed slight radioactive uptake in MCF-7 models (n = 3, Figure 4).

After imaging at 48 h, the whole lungs were removed, weighted, and measured for their radioactivity counts (Figure 5A and B). The ex vivo imaging results confirmed the in vivo imaging. Lung metastatic lesions in MDA-MB-435 had significantly higher uptake of ^{64}Cu-NOTA-YY146 than MCF-7 (7.06 ± 0.18%ID/g vs 2.17 ± 0.21%ID/g, P < 0.01). These results showed that ^{64}Cu-NOTA-YY146 could identify different CD146 expression levels in metastatic lesions.

H&E Staining.

H&E staining of the removed lung tissue verified metastatic lesions (Figure 5C). The collection of lung images showed that scattered small nodular metastases could be seen on the surface of the lung. H&E staining results displayed several tumor lesions located around the edge of the lung tissue. Tumor cells were grown in clusters, with irregular cell morphology, deeply stained nuclei, mitotic images, and obvious atypia.

Tissue Immunofluorescent Staining.

MDA-MB-435 and MCF-7 tumors from orthotopic models were collected for immunofluorescent staining of CD146 expression. MDA-MB-435 tumor tissues showed strong CD146 expression (green signals), whereas the MCF-7 tumor showed weak signals (Figure 6). The expression of CD31 (red signals), a vessel marker, was similar in both tumors. The immunofluorescent staining results verified the CD146 expression level in tumors.

DISCUSSION

Breast cancer has obvious individual differences in pathological morphology, molecular immunophenotype, and tumor biological behavior because of its highly heterogeneous

nature. Patients of different subtypes will respond differently to the same treatment even if the clinical stage is the same.[23] At present, detecting the expression of ER, PR, and HER2 before treatment can help predict prognosis and promote the development of more personalized treatment plans that are more beneficial to patients.[24] As far as we know, CD146 is associated with the poor prognosis of breast cancer and generally highly expressed in high-grade, ER negative, PR negative, or triple negative breast cancer.[11] Studies had shown that about 63.9% of TNBC patients had a high level of CD146 expression compared to other molecular subtypes.[25] In our study, we successfully applied a ^{64}Cu-NOTA-YY146 radioactive tracer to visualize the differential CD146 expression in orthotopic and lung metastatic murine tumor models by immunoPET and PET/CT imaging methods.

Molecular imaging is a highly repeatable, safe, and noninvasive imaging technique that has been widely used in the diagnosis, staging, prognosis prediction, and efficacy evaluation of various malignant tumors, including breast cancer, which is an ideal method for identifying breast cancer subtypes.[2,26] Compared to other imaging methods, immunoPET is currently the most promising molecular imaging method and combines high specificity, affinity, and antibody sensitivity. It is expected to be widely used to enable clinicians not only to see the location of tumors in vivo but also to visualize the expression, activity, and biological processes of specific molecules.[4,8] Previous studies have shown that immunoPET imaging of ^{89}Zr-labeled trastuzumab can characterize the HER2 status of breast cancer patients. ^{89}Zr-trastuzumab PET/CT imaging was positive in 88.2% of HER2 positive (30/34) patients and negative in 93.7% of HER2 negative (15/16) patients.[27] ^{89}Zr-trastuzumab could detect unsuspected HER2 positive metastases in patients with HER2 negative breast cancer.[28] The evaluation of HER2 expression has limited value for negative patients, especially for TNBC patients. Therefore, it is necessary to find better targets and probes for these patients.

CD146 has been found to participate in the growth and spread of tumors in melanoma, pancreatic cancer, renal cancer, prostate cancer, lung cancer, hepatocellular cancer, breast cancer, and other malignant tumors, which relates to poor prognosis because of high proliferation rates and high dissemination capacity.[10,16] Overexpression of CD146 in various malignant tumors has been considered as a hallmark of cancer and relates to tumor progression and poor treatment outcome.[25] The most important role of CD146 in breast cancer is to participate in epithelial-mesenchymal transition (EMT), which plays an important role in the process of tumor dissemination and metastasis.[29,30] Tumor cells undergoing EMT have tremendous changes in morphology, gaining the invasive ability and migration function, and the expression level of epithelial cell adhesion molecule (EpCAM) is reduced.[29] EMT can allow tumor cells to infiltrate blood vessels to become circulating tumor cells (CTCs), inducing distant metastases.[31]

High expression of CD146 is more common in breast cancer tissues of high-grade, high-metastatic potential, and younger patients. Approximately 11% of primary breast cancers and 63.9% of TNBC express CD146. Patients with positive CD146 expression have shorter MFS and OS and have a poorer prognosis.[25] The level of CD146 expression was also closely associated with chemotherapy resistance.[32] Liang et al. found that CD146 was involved in tamoxifen resistance in breast cancer.[13] The evaluation of CD146 at the living level can allow for early and specific diagnosis of high-grade breast cancer (especially TNBC) while

also have a certain predictive effect on prognosis and drug resistance. Our study showed that MDA-MB-435 tumor-bearing mice, which had high CD146 expression, could be visualized clearly with high radioactive uptake after the injection of ^{64}Cu-NOTA-YY146, whereas MCF-7 tumor-bearing models displayed near background uptake in vivo all of the time. At the same time, ^{64}Cu-NOTA-YY146 could achieve specific uptake of metastases through PET/CT imaging. Therefore, the tumor uptake of ^{64}Cu-NOTA-YY146 was positively correlated with the expression level of CD146.

YY146 is a mAb developed by our team that specifically targets CD146 and has been applied to immunoPET imaging of various tumors.[15–19] In melanoma-related research, ^{89}Zr-Df-YY146 and IR700-YY146 were synthesized as a radioactive tracer and photoimmunotherapy (PIT) therapeutic agent, respectively.[15] In the A375 melanoma cell line tumor model with high expression of CD146, the highest tumor uptake was obtained at 72 h p.i. of ^{89}Zr-Df-YY146 (26.48 ± 3.28%ID/g), with an unspecific tracer ^{89}Zr-Df-IgG recording a value of only 4.8 ± 1.75%ID/g. PIT reduced glucose metabolism and CD146 expression because of the generation of reactive oxygen species, which effectively inhibited tumor growth. In the study of hepatocellular carcinoma, ^{89}Zr-Df-YY146-ZW800, a dualmodal imaging agent, was synthesized, which can simultaneously perform PET and near-infrared fluorescence imaging.[16] There was an obvious and persistent accumulation of tracers in HepG2 tumors with high CD146 expression, and the T/NT ratio was significantly higher than CD146 negative Huh7 tumors. YY146 had adequate imaging effects in the xenograft tumor models of glioblastoma implanted under the skin.[8,19] These studies have shown that YY146 has high affinity, specificity, and stability for CD146 in vivo, which is consistent with our results. Our study obtained high-quality images with steady and specific tumor uptake of ^{64}Cu-NOTA-YY146 in CD146 overexpressed breast cancer xenograft tumor models.

We prepared ^{64}Cu-NOTA-YY146 for immunoPET imaging in breast cancer tumor models. The half-life time of ^{64}Cu is 12.7 h, and the emission positron abundance and energy of the nuclide are 18% and 0.65 MeV, respectively.[33] The radioactive tracers had high radiochemical purity and specific activity and were suitable for immunoPET research in vivo. The imaging results displayed that YY146 had significantly high uptake in tumors with the high CD146 expression, whereas the uptake in CD146 weaker expression models was close to the background, indicating that ^{64}Cu-NOTA-YY146 could specifically evaluate the expression level of CD146 in breast cancer at in vivo level. It could provide help for the formulation of clinical treatment plans and evaluation of treatment effects and even predict the degree of malignancy and drug resistance of breast cancer. Based on our team's research of lung cancer, glioblastoma, melanoma, and hepatocellular carcinoma,[15–19] it has been found that radionuclide or fluorescently labeled YY146 has certain therapeutic effects, which gives us some hints. In the future, we can choose therapeutic radionuclides such as ^{177}Lu to label YY146 for the treatment of breast cancer patients, providing a new treatment method for patients who are not sensitive to chemotherapy.

CONCLUSION

In this study, immunoPET imaging was performed in orthotopic breast cancer xenograft tumor models using ^{64}Cu-labeled YY146, which specifically targeted CD146. The imaging results showed that the tumor uptake of ^{64}Cu-NOTA-YY146 was specific in orthotopic models. Moreover, ^{64}Cu-NOTA-YY146 can also be effectively used to visualize lung metastatic lesions with specific radioactive uptake. ^{64}Cu-NOTA-YY146 might be potentially used for diagnosis, staging, prognosis prediction, and efficacy evaluation in breast cancer, especially TNBC and drug resistant breast cancer.

ACKNOWLEDGMENTS

This work was supported by the University of Wisconsin—Madison, the National Institutes of Health (P30CA014520), the National Natural Science Foundation of China (81871385, 81822037, 81972446, 81672602), PKU medicine-X Youth Program (PKU2020LCXQ007), Open Funding Project of the State Key Laboratory of Biochemical Engineering (2020KF-01), and Beijing Science Foundation for Distinguished Young Scholars (JQ19028).

REFERENCES

(1). Siegel RL, Miller KD, and Jemal A (2020) Cancer statistics, 2020. Ca-Cancer J. Clin 70, 7–30. [PubMed: 31912902]

(2). Wellings E, Vassiliades L, and Abdalla R (2016) Breast Cancer Screening for High-Risk Patients of Different Ages and Risk - Which Modality Is Most Effective? Cureus 8, e945. [PubMed: 28133583]

(3). Ozmen N, Dapp R, Zapf M, Gemmeke H, Ruiter NV, and van Dongen KW (2015) Comparing different ultrasound imaging methods for breast cancer detection. IEEE Trans Ultrason Ferroeiectr Freq Control 62, 637–46.

(4). Alcantara D, Leal MP, Garcia-Bocanegra I, and Garcia-Martin ML (2014) Molecular imaging of breast cancer: present and future directions. Front. Chem 2, 112. [PubMed: 25566530]

(5). Jafari SH, Saadatpour Z, Salmaninejad A, Momeni F, Mokhtari M, Nahand JS, Rahmati M, Mirzaei H, and Kianmehr M (2018) Breast cancer diagnosis: Imaging techniques and biochemical markers. J. Cell. Physiol 233, 5200–5213. [PubMed: 29219189]

(6). Medina-Ornelas S, Garcia-Perez F, Estrada-Lobato E, and Ochoa-Carrillo F (2020) ^{68}Ga-PSMA PET/CT in the evaluation of locally advanced and metastatic breast cancer, a single center experience. Am. J. Nucl. Med. Mol. Imaging 10, 135–142. [PubMed: 32704404]

(7). Knowles SM, and Wu AM (2012) Advances in immuno-positron emission tomography: antibodies for molecular imaging in oncology. J. Clin. Oncol 30, 3884–92. [PubMed: 22987087]

(8). Kang L, Li C, Rosenkrans ZT, Engle JW, Wang R, Jiang D, Xu X, and Cai W (2020) Noninvasive evaluation of CD20 expression using (64)Cu-labeled F(ab')2 fragments of obinutuzumab in lymphoma. J. Nucl. Med, jnumed.120.246595.

(9). Adams H, van de Garde EM, van Moorsel CH, Vugts DJ, van Dongen GA, Grutters JC, and Keijsers RG (2019) [^{89}Zr]Zr-rituximab PET/CT activity in patients with therapy refractory interstitial pneumonitis: a feasibility study. Am. J. Nucl. Med. Mol. Imaging 9, 296–308. [PubMed: 31976159]

(10). Nollet M, Stalin J, Moyon A, Traboulsi W, Essaadi A, Robert S, Malissen N, Bachelier R, Daniel L, Foucault-Bertaud A, et al. (2017) A novel anti-CD146 antibody specifically targets cancer cells by internalizing the molecule. Oncotarget 8, 112283–112296. [PubMed: 29348825]

(11). Zabouo G, Imbert AM, Jacquemier J, Finetti P, Moreau T, Esterni B, Birnbaum D, Bertucci F, and Chabannon C (2009) CD146 expression is associated with a poor prognosis in human breast tumors and with enhanced motility in breast cancer cell lines. Breast Cancer Res. 11, R1. [PubMed: 19123925]

(12). Velikyan I, Schweighöfer P, Feldwisch J, Seemann J, Frejd FY, Lindman H, and Sörensen J (2019) Diagnostic HER2-binding radiopharmaceutical, [^{68}Ga]Ga-ABY-025, for routine clinical use in breast cancer patients. Am. J. Nucl. Med. Mol. Imaging 9, 12–23. [PubMed: 30911434]

(13). Liang YK, Zeng, Xiao YS, Wu Y, Ouyang YX, Chen M, Li YC, Lin HY, Wei XL, Zhang YQ, et al. (2017) MCAM/ CD146 promotes tamoxifen resistance in breast cancer cells through induction of epithelial-mesenchymal transition, decreased ERalpha expression and AKT activation. Cancer Lett. 386, 65–76. [PubMed: 27838413]

(14). Tripathi SC, Fahrmann JF, Celiktas M, Aguilar M, Marini KD, Jolly MK, Katayama H, Wang H, Murage EN, Dennison JB, et al. (2017) MCAM Mediates Chemoresistance in Small-Cell Lung Cancer via the PI3K/AKT/SOX2 Signaling Pathway. Cancer Res. 77, 4414–4425. [PubMed: 28646020]

(15). Wei W, Jiang D, Ehlerding EB, Barnhart TE, Yang Y, Engle JW, Luo QY, Huang P, and Cai W (2019) CD146-Targeted Multimodal Image-Guided Photoimmunotherapy of Melanoma. Adv. Sci. (Weinh) 6, 1801237. [PubMed: 31065511]

(16). Hernandez R, Sun H, England CG, Valdovinos HF, Ehlerding EB, Barnhart TE, Yang Y, and Cai W (2016) CD146-targeted immunoPET and NIRF Imaging of Hepatocellular Carcinoma with a Dual-Labeled Monoclonal Antibody. Theranostics 6, 1918–33. [PubMed: 27570560]

(17). Sun H, England CG, Hernandez R, Graves SA, Majewski RL, Kamkaew A, Jiang D, Barnhart TE, Yang Y, and Cai W (2016) ImmunoPET for assessing the differential uptake of a CD146-specific monoclonal antibody in lung cancer. Eur. J. Nucl. Med. Mol. Imaging 43, 2169–2179. [PubMed: 27342417]

(18). Hernandez R, Sun H, England CG, Valdovinos HF, Barnhart TE, Yang Y, and Cai W (2016) ImmunoPET Imaging of CD146 Expression in Malignant Brain Tumors. Mol. Pharmaceutics 13, 2563–70.

(19). Yang Y, Hernandez R, Rao J, Yin L, Qu Y, Wu J, England CG, Graves SA, Lewis CM, Wang P, et al. (2015) Targeting CD146 with a 64Cu-labeled antibody enables in vivo immunoPET imaging of high-grade gliomas. Proc. Natl. Acad. Sci. U. S. A 112, E6525–34. [PubMed: 26553993]

(20). Eaton SL, Hurtado ML, Oldknow KJ, Graham LC, Marchant TW, Gillingwater TH, Farquharson C, and Wishart TM (2014) A guide to modern quantitative fluorescent western blotting with troubleshooting strategies. J. Visualized Exp 93, e52099.

(21). England CG, Ehlerding EB, Hernandez R, Rekoske BT, Graves SA, Sun H, Liu G, McNeel DG, Barnhart TE, and Cai W (2017) Preclinical Pharmacokinetics and Biodistribution Studies of 89Zr-Labeled Pembrolizumab. J. Nucl. Med 58, 162–168. [PubMed: 27493273]

(22). Kang L, Jiang D, England CG, Barnhart TE, Yu B, Rosenkrans ZT, Wang R, Engle JW, Xu X, Huang P, et al. (2018) ImmunoPET imaging of CD38 in murine lymphoma models using (89)Zr-labeled daratumumab. Eur. J. Nucl. Med. Mol. Imaging 45, 1372–1381. [PubMed: 29450576]

(23). The Cancer Genome Atlas Network. (2012) Comprehensive molecular portraits of human breast tumours. Nature 490, 61–70. [PubMed: 23000897]

(24). Liu H, Chen Y, Wu S, Song F, Zhang H, and Tian M (2016) Molecular imaging using PET and SPECT for identification of breast cancer subtypes. Nucl. Med. Commun 37, 1116–24. [PubMed: 27438531]

(25). de Kruijff IE, Timmermans AM, den Bakker MA, Trapman-Jansen A, Foekens R, Meijer-Van Gelder ME, Oomende Hoop E, Smid M, Hollestelle A, and van Deurzen CHM (2018) The Prevalence of CD146 Expression in Breast Cancer Subtypes and Its Relation to Outcome. Cancers 10, 134.

(26). Soldevilla-Gallardo I, Medina-Ornelas SS, Villarreal-Garza C, Bargallo-Rocha E, Caro-Sanchez CH, Hernandez-Ramirez R, and Estrada-Lobato E (2018) Usefulness of positron emission mammography in the evaluation of response to neoadjuvant chemotherapy in patients with breast cancer. Am. J. Nuci. Med. Mol. Imaging 8, 341–350.

(27). Dehdashti F, Wu N, Bose R, Naughton MJ, Ma CX, Marquez-Nostra BV, Diebolder P, Mpoy C, Rogers BE, Lapi SE, et al. (2018) Evaluation of [(89)Zr]trastuzumab-PET/CT in differentiating HER2-positive from HER2-negative breast cancer. Breast Cancer Res. Treat 169, 523–530. [PubMed: 29442264]

(28). Ulaner GA, Hyman DM, Ross DS, Corben A, Chandarlapaty S, Goldfarb S, McArthur H, Erinjeri JP, Solomon SB, Kolb H, et al. (2016) Detection of HER2-Positive Metastases in Patients with HER2-Negative Primary Breast Cancer Using 89Zr-Trastuzumab PET/CT. J. Nucl. Med 57, 1523–1528. [PubMed: 27151988]

(29). Hyun KA, Koo GB, Han H, Sohn J, Choi W, Kim SI, Jung HI, and Kim YS (2016) Epithelial-to-mesenchymal transition leads to loss of EpCAM and different physical properties in circulating tumor cells from metastatic breast cancer. Oncotarget 7, 24677–87. [PubMed: 27013581]

(30). Kebir A, Harhouri K, Guillet B, Liu JW, Foucault-Bertaud A, Lamy E, Kaspi E, Elganfoud N, Vely F, Sabatier F, et al. (2010) CD146 short isoform increases the proangiogenic potential of endothelial progenitor cells in vitro and in vivo. Circ. Res 107, 66–75. [PubMed: 20448216]

(31). Yu M, Bardia A, Wittner BS, Stott SL, Smas ME, Ting DT, Isakoff SJ, Ciciliano JC, Wells MN, Shah AM, et al. (2013) Circulating breast tumor cells exhibit dynamic changes in epithelial and mesenchymal composition. Science 339, 580–4. [PubMed: 23372014]

(32). Zeng D, Liang YK, Xiao YS, Wei XL, Lin HY, Wu Y, Bai JW, Chen M, and Zhang GJ (2020) Inhibition of Notch1 reverses EMT and chemoresistance to cisplatin via direct down-regulation of MCAM in triple-negative breast cancer cells. Int. J. Cancer 147, 490–504. [PubMed: 32020593]

(33). Fu R, Carroll L, Yahioglu G, Aboagye EO, and Miller PW (2018) Antibody Fragment and Affibody ImmunoPET Imaging Agents: Radiolabelling Strategies and Applications. ChemMedChem 13, 2466–2478 [PubMed: 30246488]

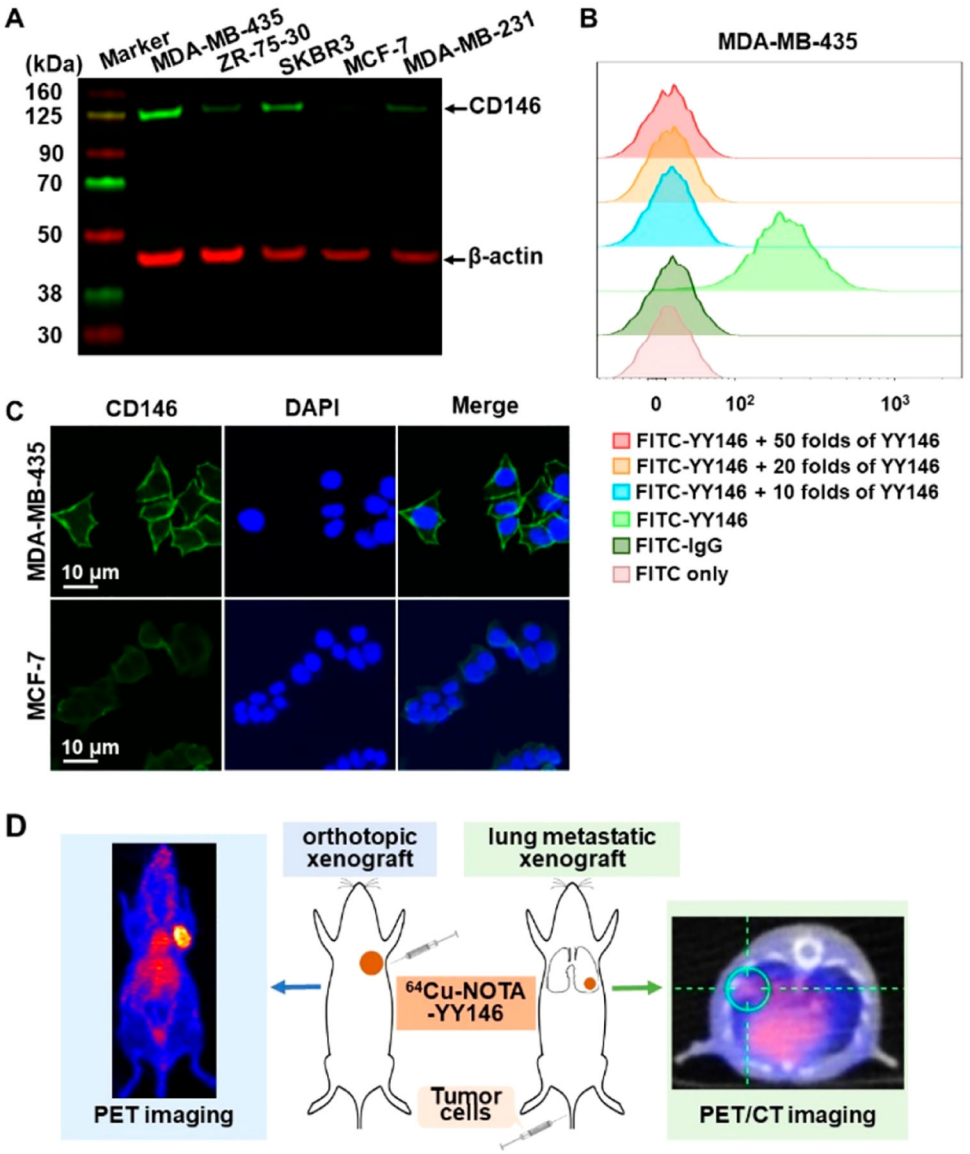

Figure 1.

Screening of CD146 expression at the cellular level and schematic diagram.

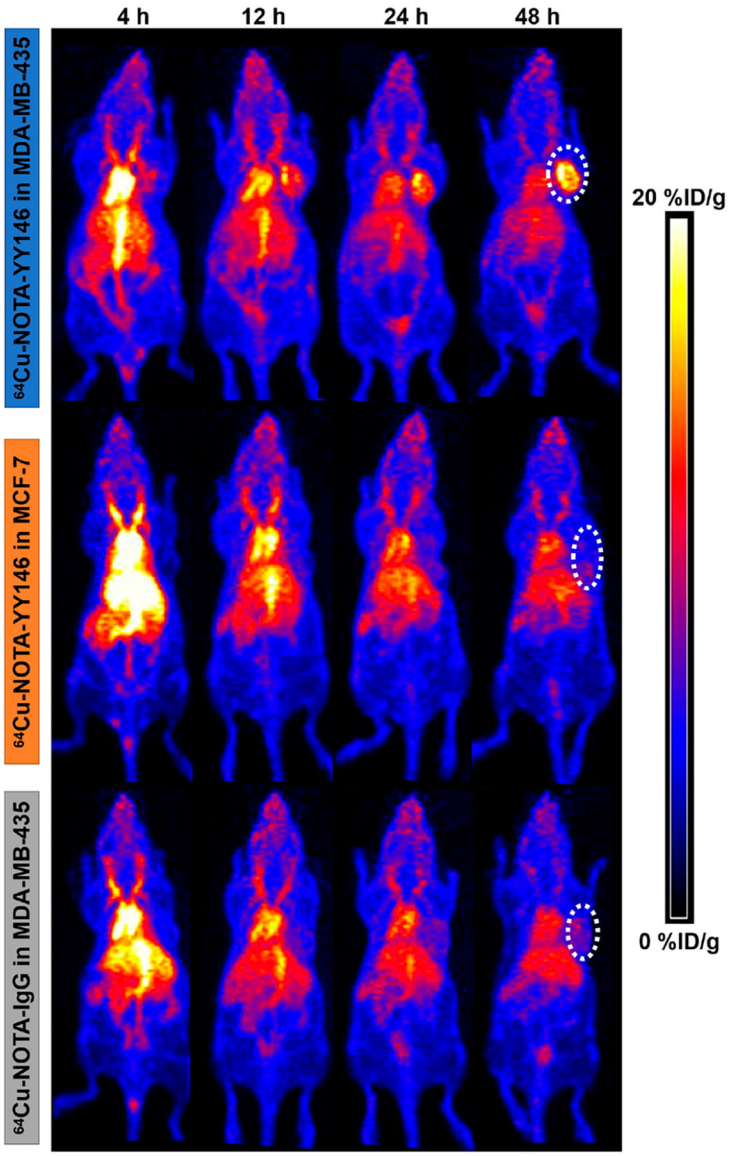

Figure 2.
^{64}Cu-NOTA-YY146 PET imaging in MDA-MB-435 and MCF-7 orthotopic tumor models.

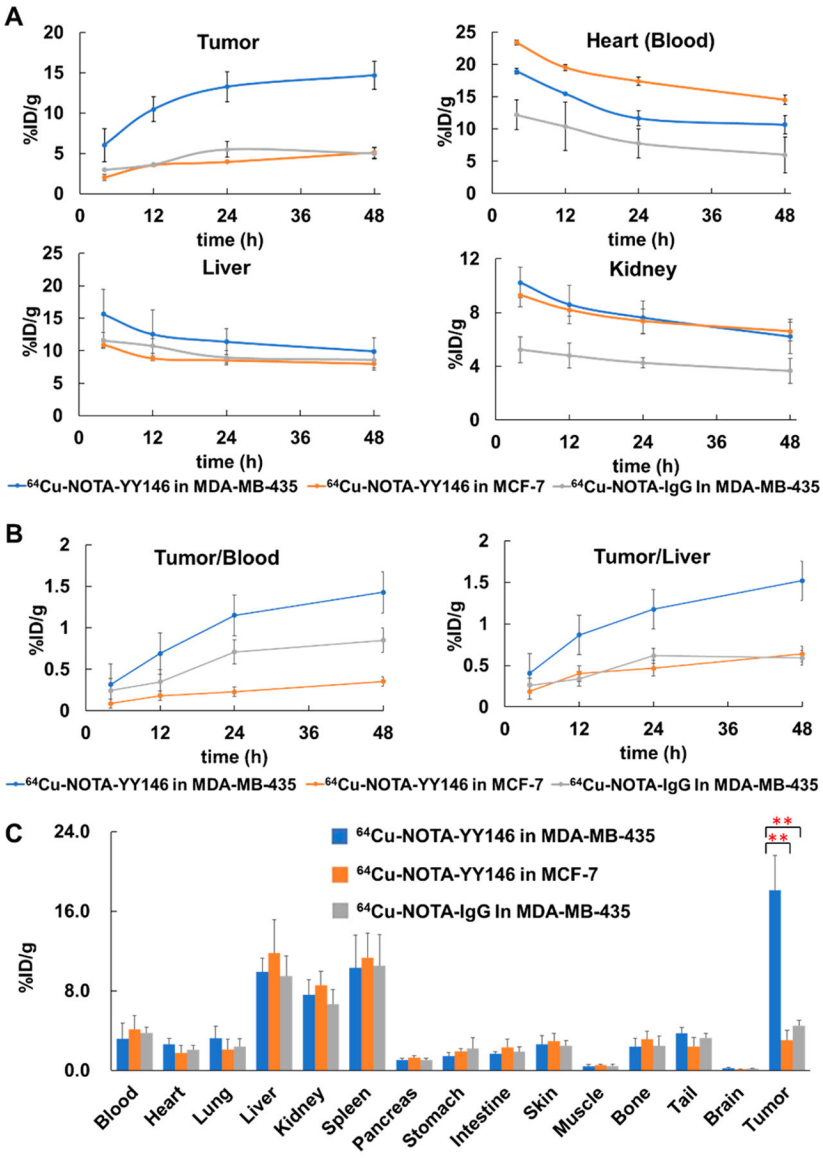

Figure 3.

Semiquantitative analysis and biodistribution of ^{64}Cu-NOTA-YY146 in orthotopic tumor models.

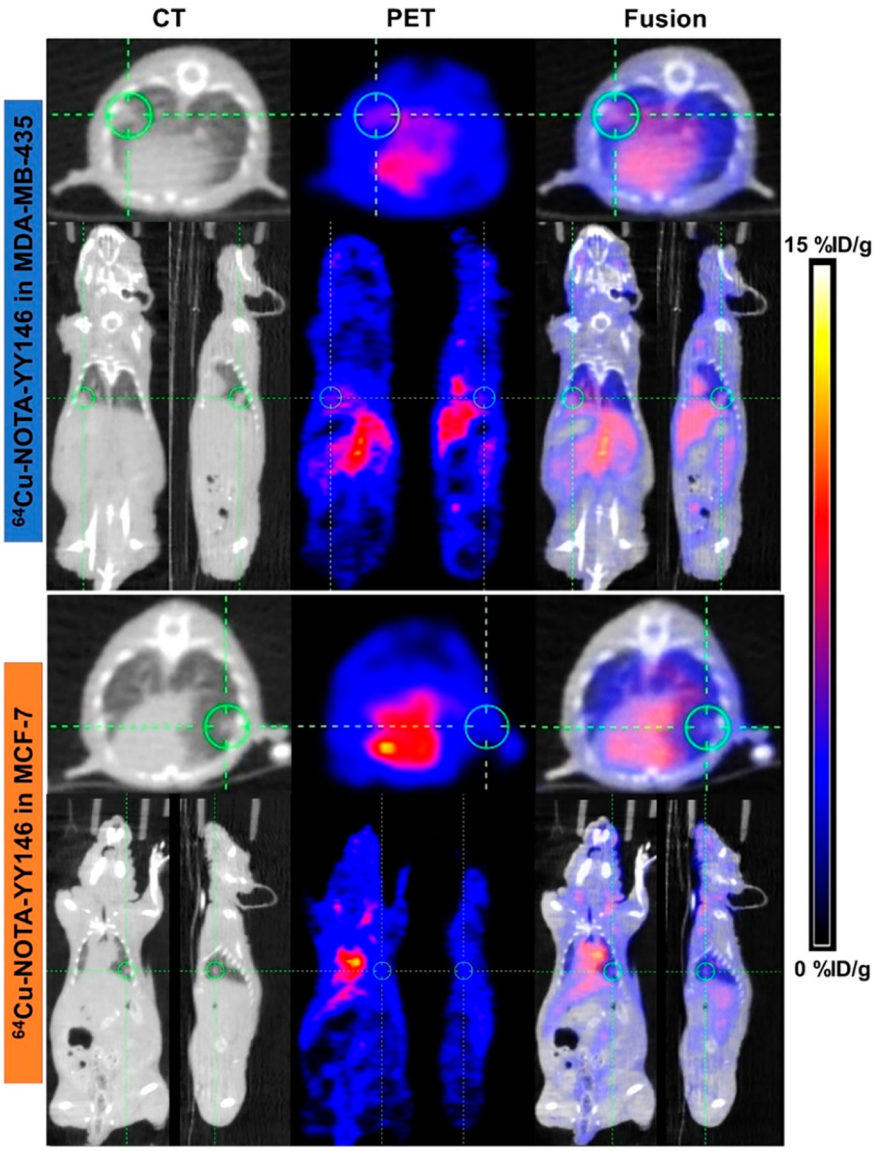

Figure 4.

PET/CT imaging of lung metastatic tumor models at 48 h after the injection of ^{64}Cu-NOTA-YY146.

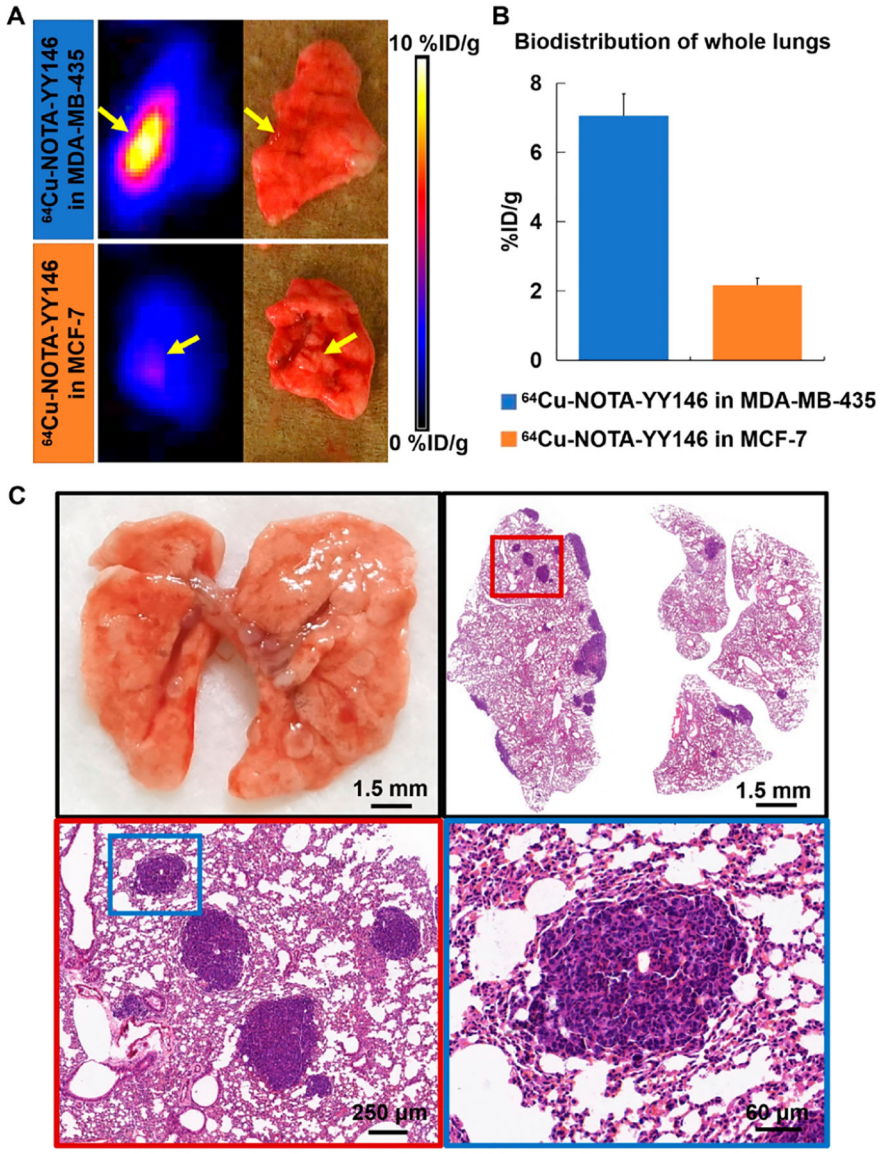

Figure 5.

Ex vivo imaging, biodistribution, and H&E staining of metastatic lungs.

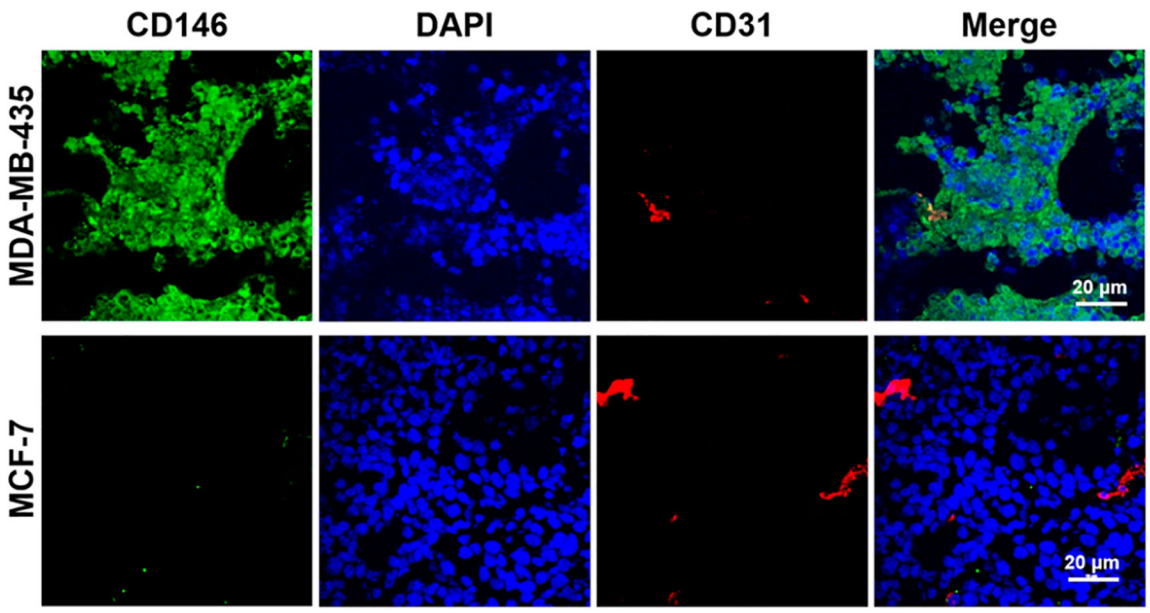

Figure 6.
Tissue immunofluorescent staining of CD146 and CD31 of orthotopic tumors.